JBC RESEARCH ARTICLE

E41K mutation activates Bruton's tyrosine kinase by stabilizing an inositol hexakisphosphate-dependent invisible dimer

Received for publication, January 24, 2024, and in revised form, June 19, 2024 Published, Papers in Press, July 4, 2024,
https://doi.org/10.1016/j.jbc.2024.107535

Subhankar Chowdhury[1,‡], **Manas Pratim Chakraborty**[1,‡], **Swarnendu Roy**[1,‡], **Bipra Prasad Dey**[1], **Kaustav Gangopadhyay**[1], **and Rahul Das**[1,2,*]

From the [1]*Department of Biological Sciences, and* [2]*Centre for Advanced Functional Materials, Indian Institute of Science Education and Research Kolkata, Mohanpur, India*

Reviewed by members of the JBC Editorial Board. Edited by Alex Toker

Bruton's tyrosine kinase (BTK) regulates diverse cellular signaling of the innate and adaptive immune system in response to microbial pathogens. Downregulation or constitutive activation of BTK is reported in patients with autoimmune diseases or various B-cell leukemias. BTK is a multidomain protein tyrosine kinase that adopts an Src-like autoinhibited conformation maintained by the interaction between the kinase and PH-TH domains. The PH-TH domain plays a central role in regulating BTK function. BTK is activated by binding to PIP_3 at the plasma membrane upon stimulation by the B-cell receptor (BCR). The PIP_3 binding allows dimerization of the PH-TH domain and subsequent transphosphorylation of the activation loop. Alternatively, a recent study shows that the multivalent T-cell-independent (TI) antigen induces BCR response by activating BTK independent of PIP_3 binding. It was proposed that a transiently stable IP_6-dependent PH-TH dimer may activate BTK during BCR activation by the TI antigens. However, no IP_6-dependent PH-TH dimer has been identified yet. Here, we investigated a constitutively active PH-TH mutant (E41K) to determine if the elusive IP_6-dependent PH-TH dimer exists. We showed that the constitutively active E41K mutation activates BTK by stabilizing the IP_6-dependent PH-TH dimer. We observed that a downregulating mutation in the PH-TH domain (R28H) linked to X-linked agammaglobulinemia impairs BTK activation at the membrane and in the cytosol by preventing PH-TH dimerization. We conclude that the IP_6 dynamically remodels the BTK active fraction between the membrane and the cytoplasm. Stimulating with IP_6 increases the cytosolic fraction of the activated BTK.

Bruton's tyrosine kinase (BTK) is an indispensable signaling module of innate and adaptive immune response against pathogens. BTK downregulation in patients with X-linked agammaglobulinemia (XLA) causes recurring bacterial and viral infections (1–4). On the other hand, constitutive activation of BTK is often linked to several forms of B-cell leukemias and lymphomas like chronic lymphocytic leukemia (5), and diffuse large B cell lymphoma (ABC-DLBCL) (6), suggesting a critical regulatory function of BTK in B-cell development and proliferation (7). Thus, BTK has been an important pharmacological target for the treatment of various B-cell malignancies (8–10).

In macrophages, a component of innate immunity, BTK phosphorylates the Toll-like receptors to initiate an antiviral response (11). In B-cells, a component of adaptive immunity, BTK is essential for connecting the B-cell antigen receptor (BCR) activation to the downstream calcium flux (12–14). BTK is a Tec family kinase (15) that shares a homologous structural architecture with the Src kinases, where the kinase domain is flanked by two N-terminal Src homology domains, SH3 and SH2 (Fig. 1*A*) (16–18). BTK has an additional lipid binding pleckstrin homology (PH) domain fused to the Tec homology (TH) domain at the N-terminal of the SH3 domain (19, 20). Unlike Src kinase, where the autoinhibited conformation is stabilized by the C-terminal phosphotyrosine residue (16–18), in BTK, the PH-TH domain functions as the negative regulator (21–23). In the autoinhibited state, the SH3 and SH2 domains assemble at the back of the kinase domain (Fig. 1*B*) (16–18, 22). The interaction of the PH-TH domain and the kinase domain maintains the autoinhibited structure, blocking the activation loop face of the kinase domain, which occludes the lipid binding to the PH-TH domain (22, 24, 25).

Antigen binding to BCR activates BTK by recruiting kinase to the plasma membrane (Fig. S1*A*) (26, 27). The localization of the BTK to the membrane is mediated by the binding between the phosphatidylinositol (3,4,5)-triphosphate (PIP_3) and the canonical lipid-binding site of the PH-TH domain (Fig. S1*A*) (4, 22, 28, 29). Binding to PIP_3 removes the inhibitory interaction, allowing BTK to dimerize (28, 30) and rapidly phosphorylate the tyrosine residue in the activation loop (13, 31, 32). The PIP_3 induces dimerization of the PH-TH domain (called Saraste dimer) where hydrophobic dimer interfaced (called Saraste interface) is constituted by α1-helix, β1 and β3-β4 loop (22, 28, 29). At the membrane, the PH-TH dimer is stabilized by a second PIP_3 binding to the peripheral lipid binding site (Fig. S1*A*), which imparts a switch-like property to the kinase (30).

‡ These authors contributed equally to this work.
* For correspondence: Rahul Das, rahul.das@iiserkol.ac.in.

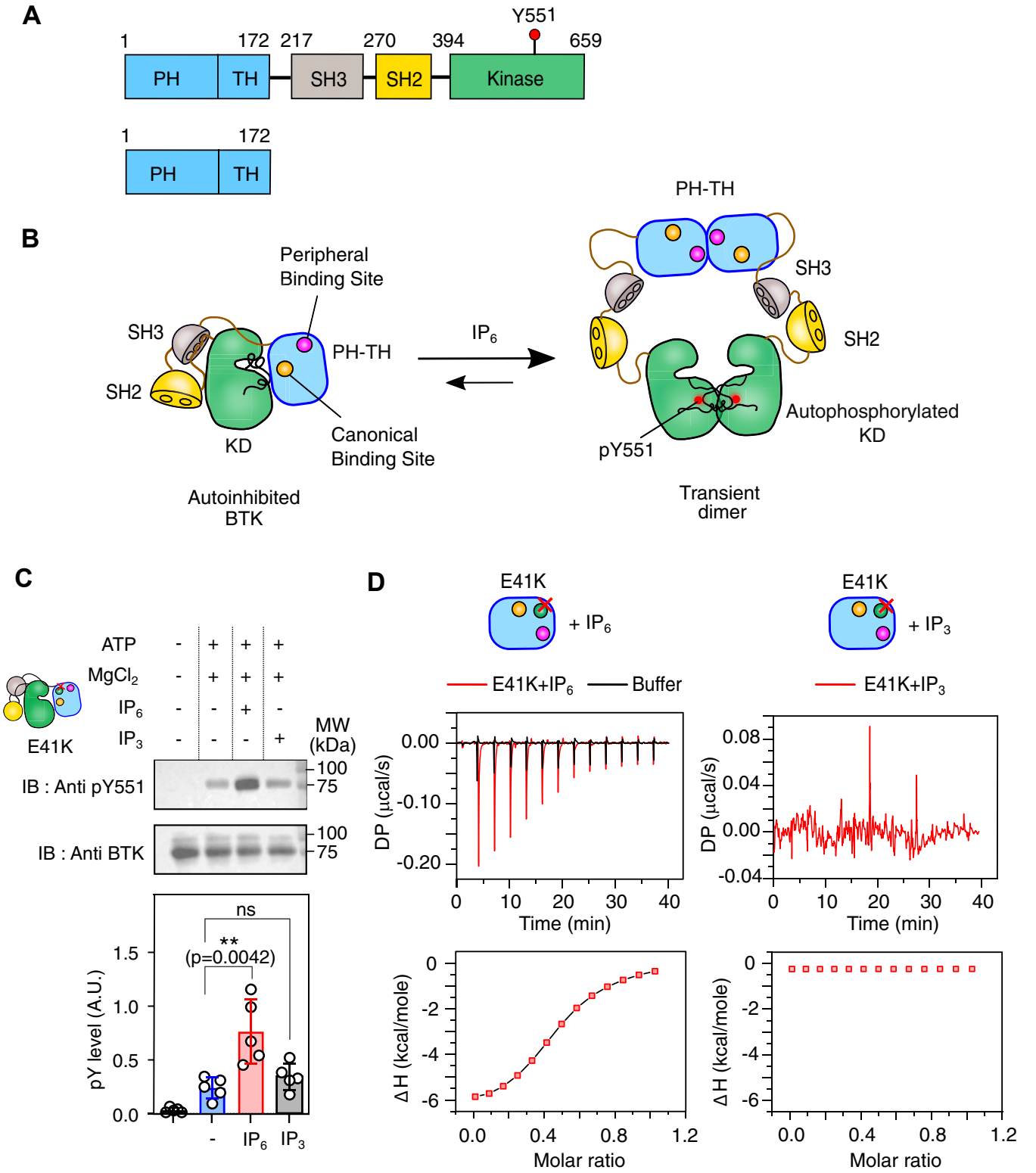

Figure 1. Activation of BTK E41K mutant by Inositol Hexakisphosphate (IP_6). *A*, schematic representation of domain architecture of Bruton's Tyrosine Kinase and PH-TH domain used in this study. *B*, mechanism of Inositol Hexakisphosphate (IP_6) dependent activation of Bruton's Tyrosine Kinase (22). *C*, *top panel*: representative immunoblot of Y551 autophosphorylation in the full-length BTK E41K (2 µM) mutant with 100 µM IP_6 or IP_3. *Bottom panel*: densitometric analysis of the immunoblots of BTK E41K mutant activated with IP_6 or IP_3. The error bar represents standard deviations from five independent experiments. Data are presented as mean values ± SD from five independent experiments. Data analyses were performed using GraphPad Prism version 9.5.1. An unpaired two-tailed *t* test was used to calculate significance. *D*, *top panel*: Isothermal Titration Calorimetric (ITC) measurement of IP_6 (left) or IP_3 (right) binding to E41K mutant of an isolated PH-TH domain. For each titration, 25 µM of PH-TH^{E41K} was titrated with 137 µM of ligand. Bottom panel: solid line represents the two-site independent binding fitting of the ITC titration of IP_6 and indicated PH-TH domain. The experimental points are indicated in red square. The ITC titration of IP_3 and PH-TH^{E41K} domain could not be fit to any model. The plots were generated using Origin Pro 2020b.

Alternatively, recent studies showed that inositol hexakisphosphate (IP_6) is required for a T-cell-independent BCR response against bacterial and viral infection (33). Deficiency of inositol polyphosphate multikinase in mice, the enzyme that generates the precursor for IP_6 biosynthesis from inositol tetrakisphosphate (IP_4) (34), impairs BTK activity and attenuates calcium signaling in B-cells. The IP_6 was previously shown to induce BTK activation in solution by the same PH-TH Saraste dimer, where two molecules of IP_6 bind to the canonical site and peripheral sites, respectively (Fig. 1*B*) (22), suggesting IP_6 activates BTK independently of its membrane localization. Mutations that impair IP_6 binding to the peripheral sites inhibit BTK activation in the solution. However, no PH-TH dimer in solution has yet been determined. It was speculated that the PH-TH domain might form a transiently stable dimer in the presence of IP_6 (22). Therefore, the lack of evidence for an IP_6-dependent BTK dimer makes the functional relevance of T-cell-independent BCR response to pathogens uncertain.

In the present study, we focused on an E41K mutant of the PH-TH domain that activates BTK constitutively (35) and binds to IP_6 with a higher affinity than the wild-type (4). We observed that, unlike wild-type BTK (22), the E41K mutant is activated by IP_6 in solution by stabilizing a PH-TH dimer, which was otherwise invisible by most biophysical techniques due to the transient nature of the dimer. Our mutation studies suggest that the PH-TH dimerization is mediated by an alternate dimer interface, where an IP_6 molecule holds two lateral PH-TH domains together. The R28H mutation found in the canonical lipid-binding site of the PH-TH domain in patients with XLA (4, 36) prevents IP_6-dependent PH-TH dimerization and inhibits BTK activation. In cells, higher IP_6 concentration increases the cytosolic fraction of activated BTK. Finally, we presented a mechanism explaining how IP_6 remodels the equilibrium, like a switch, between the membrane fraction and cytosolic fraction of BTK in the cell.

Results and discussion

IP_6 activates BTK E41K mutant in solution

The E41K mutation is located at the β3-β4 loop of the PH-TH domain (Fig. 2*A*). The crystal structure of an isolated PH-TH^{E41K} mutant was solved in a complex with D-myo-inositol 1,3,4,5-tetra-kisphosphate (IP_4) (37). The lysine residue (at 41 position) does not directly contact the IP_4 molecule in the structure at the canonical binding site (37). Instead, the lysine creates an overall positively charged environment, allowing the second IP_4 molecule to bind, leading to spontaneous membrane recruitment of the BTK, allowing autophosphorylation of Y551 at the activation loop, and enhanced Ca^{2+} signaling (35, 37, 38). The high structural homology (RMSD of 0.43 Å) between the PH-TH^{E41K} mutant in complex with IP_4 (PDB ID: 1BWN) (37) and the wild-type PH-TH domain in complex with IP_6 (PDB ID: 4Y94) (22) does not explain the observed functional difference (Fig. S1*B*). However, a higher binding affinity of the E41K mutant for IP_6 (4) suggests that the mutation may stabilize a PH-TH dimer. To find out if IP_6 also activates BTK carrying an E41K mutation in solution, we purified the full-length BTK (denoted as BTK^{E41K}) and an isolated PH-TH domain with E41K mutant (denoted as PH-TH^{E41K}) and determined the phosphorylation of Y551 and binding of IP_6, respectively (Fig. 1, *C* and *D*). Without any ligand, we observed that the BTK^{E41K} spontaneously phosphorylated at Y551 (Fig. 1*C*). On the other hand, adding IP_6 significantly increases the Y551 phosphorylation compared to IP_3, the unliganded state, and the wild-type BTK (Fig. S1, *C* and *D*). As reported previously, IP_3 does not induce phosphorylation of Y551 because the PH-TH^{E41K} domain does not bind to IP_3 (Fig. 1, *C* and *D* and Table S1) (4). On the other hand, PH-TH^{E41K} binds to IP_6 with two distinct dissociation constants (K_{d1} = 152 ± 18 nM and K_{d2} = 1.3 ± 0.4 μM) when the ITC data was fitted to a two-site independent binding model (Fig. 1*D* and Table S1). We observed that the K_{d1} and K_{d2} represent the strong and weak IP_6 binding sites, respectively, which may correspond to the canonical and peripheral lipid binding sites in the PH-TH domain, respectively (22). We asked if the improved activation of BTK is due to the greater stability of the IP_6-dependent dimer in the solution.

IP_6 promotes PH-TH dimerization

In the crystal structure of the PH-TH domain in complex with IP_6, the Saraste-dimer interface is comprised of antiparallel interaction between the adjacent β3-β4 loop and α1-helix of each PH-TH domain (Fig. 2*A*) (22). However, due to the transient nature of the hydrophobic interaction at the Saraste-dimer interface, no IP_6-dependent PH-TH dimer has yet been detected in the solution. Since PH-TH^{E41K} binds IP_6 with a stronger affinity compared to the wild-type (4), we speculate if the activation of BTK^{E41K} is due to forming a stable IP_6-dependent PH-TH dimer. We probed the PH-TH^{E41K} dimer from the mobility of the protein by size-exclusion chromatography and from dynamic light scattering (DLS) measurements (Fig. 2). In our assays, we used double mutants (R28H and R49S at the canonical and peripheral sites, respectively) of the PH-TH domain made in the wild-type or E41K background as a monomer control. The anticipated molecular weight and theoretical hydrodynamic radius of the PH-TH dimer are 38 kDa and 3.0 nm, respectively (Fig. S2*B*). As reported, we could not detect IP_6-dependent dimers for the wild-type PH-TH domain by size-exclusion chromatography and DLS experiment (Figs. 2*D* and S2, *A*–*C*). We observed a minor shift in the retention time for the IP_6 bound PH-TH domain compared to the *apo*-state, and the hydrodynamic radius (2.18 ± 0.10 nm) was close to a monomer (Figs. 2*D* and S2, *A*–*C*).

On the contrary, the PH-TH^{E41K} in the presence of IP_6 migrated close to a dimer (44 kDa) species in a size-exclusion column (Fig. 2*B*). The hydrodynamic radius of 3.14 ± 0.48 nm suggests that the PH-TH^{E41K} in the presence of IP_6 forms a stable homodimer (Figs. 2*D* and S2, *B* and *C*). We noted that PH-TH^{E41K} does not dimerize in the *apo*-state or in the

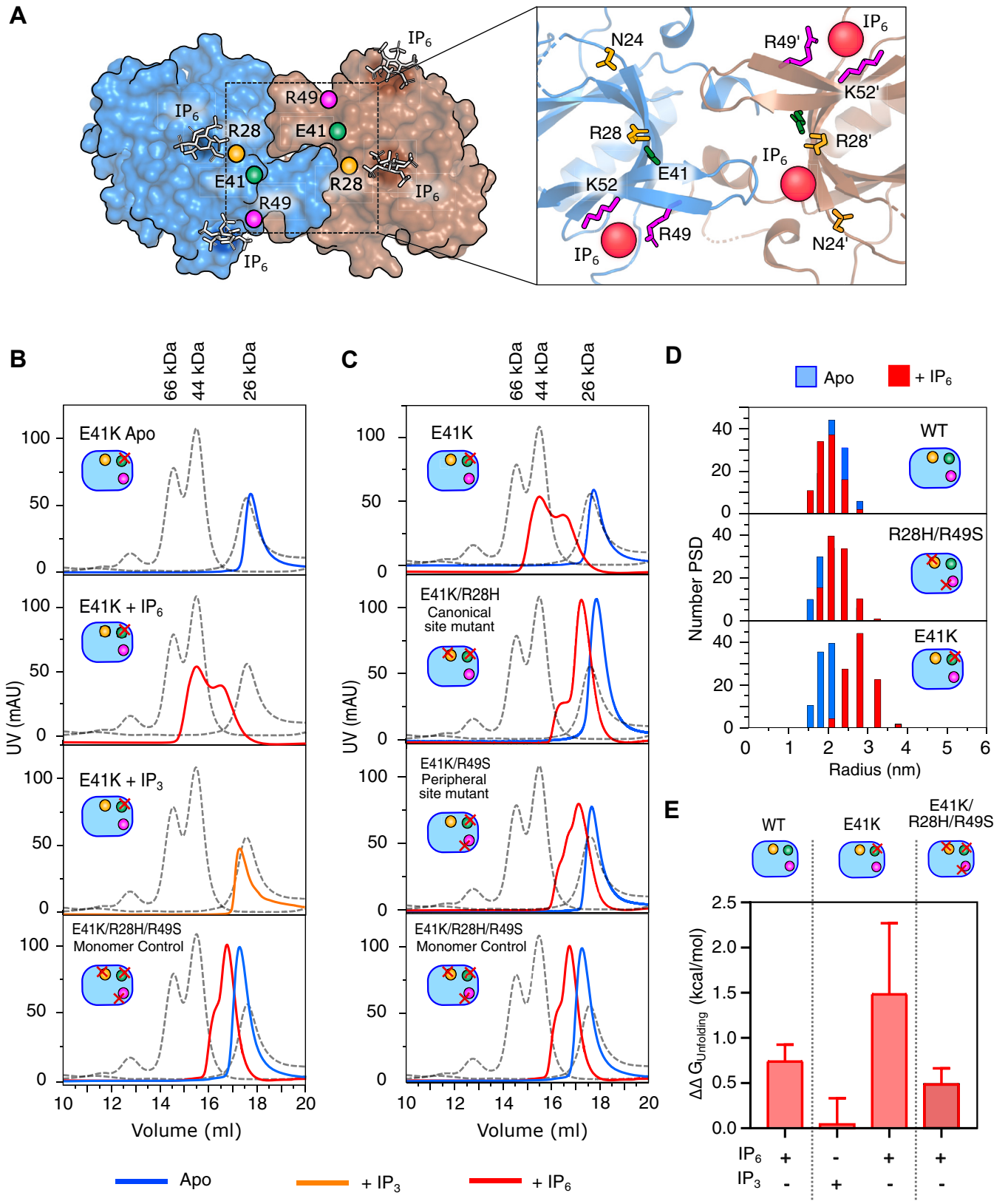

Figure 2. Probing the IP_6-dependent PH-TH dimer in solution. *A*, the space-filled model of BTK PH-TH Saraste dimer in complex with IP_6 (PDB 4Y94). The canonical and peripheral ligand binding site is shown in the inset. *B* and *C*, representative elution profiles of indicated constructs of PH-TH domain in the presence (300 μM) or absence of IP_6 or IP_3 when passed through a size-exclusion column. The triple mutant of the PH-TH domain (E41K/R28H/R49S) is used as monomer control. The dotted line represents the elution profiles of standard protein mixtures containing BSA (66 kDa), Ovalbumin (44 kDa), and ULP1 (26 kDa). The plots were generated by XMGRACE Ver 5.1.25. *D*, dynamic light scattering measurement of indicated constructs of PH-TH domain in the presence (*red bar*) or absence (*blue bar*) of IP_6. The plots were generated using Origin Pro 2020b. *E*, $\Delta\Delta G_{unfolding}$ of ligand-bound BTK PH-TH constructs derived from the thermal denaturation profile measured using a Circular Dichroism (CD) spectrophotometer (Fig. S2*D*). $\Delta\Delta G_{unfolding}$ was derived at the T_m of the respective *apo* state of indicated constructs. Data are presented as mean values ± SD from three independent experiments. The plots were generated using GraphPad Prism version 9.5.1. See Table S2 and Fig. S2.

presence of IP_3 (Fig. 2*B*). To find out if IP_6 induces structural stability in the PH-TH domain, we compare Gibbs free energy for unfolding ($\Delta G_{unfolding}$) of the PH-TH constructs derived at the melting temperature (T_m) of the respective *apo* state (Table S2) (39, 40). The T_m was determined from the thermal denaturation profile of the PH-TH domains recorded in the presence and absence of ligands (Fig. S2*D*) (39, 41). Comparison of change in $\Delta G_{unfolding}$ of the ligand-bound PH-TH constructs with respect to the corresponding apo state ($\Delta\Delta G_{unfolding} = \Delta G_{holo} - \Delta G_{apo}$), we observed that the PH-TH^{E41K} in complex with IP_6 (1.49 ± 0.79 kcal/mole) is structurally more stable than IP_3 complex or wild-type PH-TH domain (Figs. 2*E*, S2*D*, and Table S2). Our data suggests that the activating mutant stabilizes the PH-TH domain structure compared to inactivating mutants or ligands (Fig. 2*E*) (29).

Activation of BTK E41K mutant is mediated by the IP_6-dependent PH-TH dimer

The β3-β4 segment crosstalk with the canonical lipid binding site, peripheral lipid binding site, and the Saraste dimer interface. Recent studies suggest that PIP_3 binding to the canonical and peripheral lipid binding is important for membrane docking and dimerization of BTK (29, 30). Mutation, such as R28H found in patients with XLA, at canonical lipid binding pocket impairs PIP_3 binding and down-regulates BTK signaling (42). We next investigate whether the down-regulation of BTK in XLA mutants found at the PH-TH domain is due to impaired dimerization.

We begin with characterizing IP_6 binding and dimerization of the R28H mutant (at the canonical site) and R49S mutant (at the peripheral site) created in the PH-TH^{E41K} background (Figs. 2*C* and 3*A*, and Table S1). We also compared the ability to autophosphorylate full-length BTK E41K mutant (BTK^{E41K}) bearing a mutation in the canonical (R28H) or peripheral (R49S) lipid binding site (Fig. 3, *B* and *C*). We observed that the R28H mutation impairs IP_6 binding to the canonical site but retains the weak IP_6 binding to the peripheral lipid binding site with K_d of 2.4 ± 0.15 μM (Fig. 3*A* and Table S1). The R49S mutation in the peripheral lipid binding site impairs IP_6 binding at the peripheral site but retains the strong IP_6 binding to the canonical lipid binding site with K_d of 622 ± 77 nM. However, in the size-exclusion chromatography, we observed that none of the mutants dimerize in the presence of IP_6 and migrate along with the monomer control (Fig. 2*C*). As anticipated, impaired PH-TH dimerization impairs IP_6-dependent autophosphorylation of BTK^{E41K} R28H or R49S mutants (Fig. 3, *B* and *C*). Our data shows that the XLA mutation (R28H) and mutation at the peripheral lipid binding site (R49S) impair BTK function by destabilizing the Saraste dimer interface, suggesting an allosteric crosstalk between the two lipid binding pockets and the dimer interface.

E41K mutation promotes spontaneous localization of BTK to the plasma membrane

In B-cells, BTK is activated by localizing the kinase to the membrane following antigen binding to the BCR (26, 43). The E41K mutation spontaneously localizes the kinase to the plasma membrane when expressed in NIH 3T3 cells and *trans*-phosphorylate Y551 in the activation loop (13, 35, 38). At the membrane, the binding to PIP_3 at the canonical and peripheral lipid binding sites activates BTK by stabilizing the Saraste dimer (30). Recently, IP_6 was shown to regulate BTK function during BCR response to T-cell independent antigens (33). We wonder about how IP_6 may remodel the BTK activation profile at the membrane.

To study the effect of IP_6 on the activation profile of BTK, we transiently transfected wild-type and E41K mutant (BTK^{E41K}) of BTK-tagged mCherry to the CHO cells and determined the membrane localization (Fig. 4, *A* and *B*). The plasma membrane was marked with Wheat Germ Agglutinin (WGA) fused to Alexa 633 (44). The activation of BTK was determined with a specific anti-pY551 antibody and then imaged by labeling with a FITC-tagged secondary antibody (Fig. 4). The membrane localization of BTK^{E41K} was estimated from the quantification of Pearson's colocalization coefficient (PCC) of mCherry and Alexa 633 (45). A higher PCC value indicates higher membrane localization. We used a triple mutant (E41K, R28H, and R49S) of BTK as a monomer control (negative control) (Fig. S3, *B*–*D*). We observed that a major fraction of wild-type BTK remains in the cytosol (Fig. 4*A*). In contrast, a significant portion of the BTK^{E41K} localized to the plasma membrane (Fig. 4*B*). Consistent with our *in-vitro* experiments (Figs. 2 and 3), we observed that the mutation at the peripheral lipid binding site (R49S), made in the background of BTK^{E41K}, can spontaneously localize to the membrane (Fig. 4*C*). We observed that a minor fraction of BTK$^{E41K/R49S}$ peripheral site mutant is also present in cytosol (Figs. 4*C* and S4*C*). However, the XLA mutation (R28H) impairs the membrane localization of BTK^{E41K} (Fig. 4*D*). As shown previously, we also observed that only the BTK^{E41K} and a minor fraction of BTK$^{E41K/R49S}$ spontaneously phosphorylated Y551 at the plasma membrane (Figs. 4, *B* and *C*, 5*A*, and S3, *B* and *C*), but none of the other two mutants were active (13, 35, 38). These data suggest that the BTK in the CHO cells is mainly recruited to the membrane by binding PIP_3 to the canonical lipid-binding site of the PH-TH domain (29, 30, 38). The binding of PIP_3 to the peripheral lipid binding site is required for the transphosphorylation of BTK (22, 30). We asked if BTK^{E41K} is activated only at the plasma membrane or if IP_6 could stimulate the cytoplasmic fraction of BTK^{E41K}.

IP_6 increases the cytosolic fraction of active BTK

Next, we focused on how the BTK^{E41K} activation profile at the membrane may be remodeled upon stimulating the transiently transfected CHO cells with IP_6. Our NMR analysis of CHO cells treated with and without IP_6 suggests that the IP_6 spontaneously enters the cell (Fig. S3*E*). We consider that the IP_6 may enter the cell through pinocytosis (46) and transphosphorylate Y551 of BTK^{E41K} by inducing an IP_6-dependent dimerization (30). In Figure 4, *A*–*D*, Figs. S3B, and S4, mCherry intensity indicates BTK expression level, FITC indicates the level of Y551 phosphorylation, and WGA-Alexa

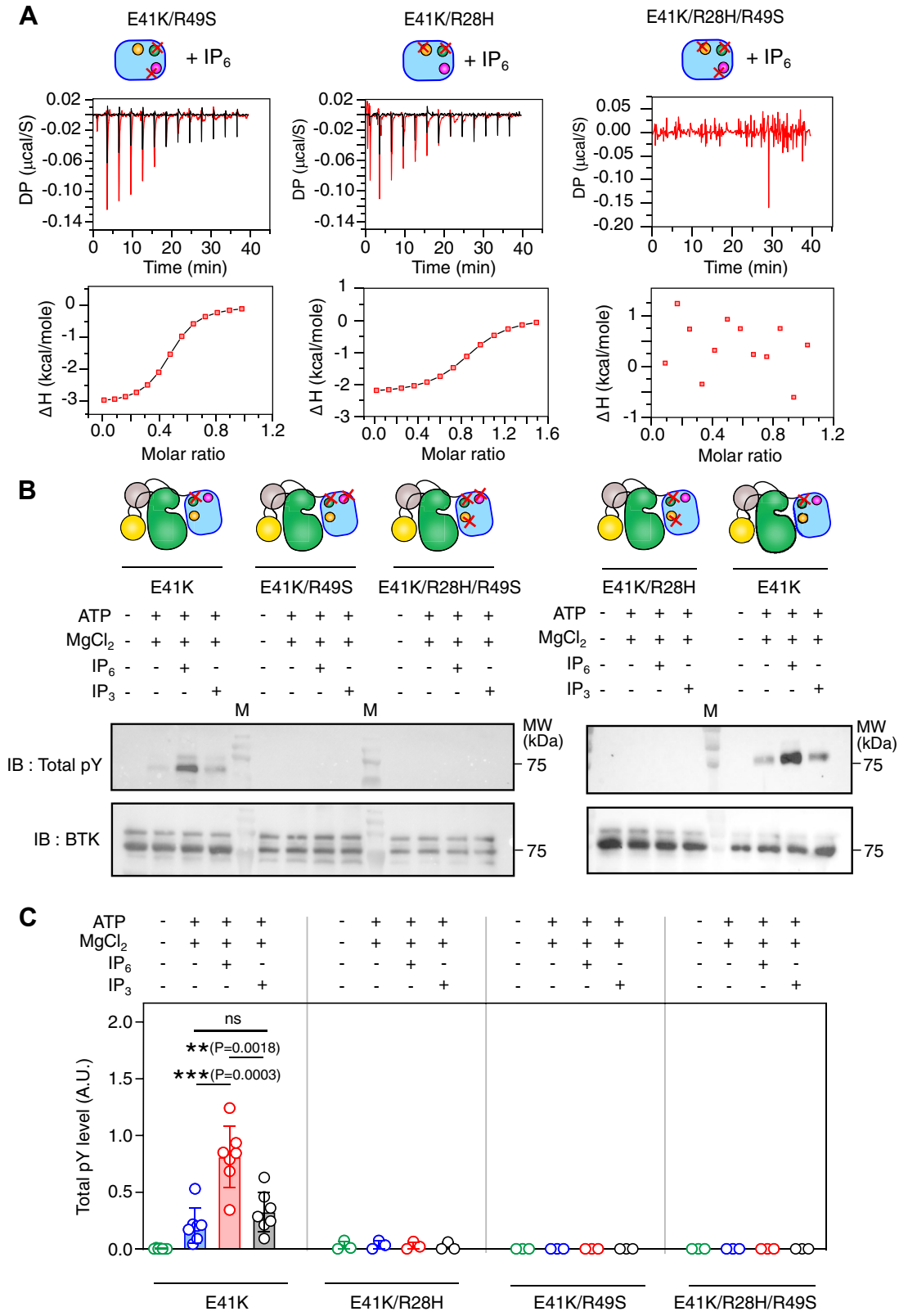

Figure 3. Functional analysis of IP_6 mediated activation of BTK E41K mutant. *A*, ITC titration of IP_6 to the indicated mutants of the PH-TH domain of BTK. For each titration, 25 µM of PH-TH^{E41K} was titrated with 137 µM of ligand. *Top panel*: *red lines* indicate protein and ligand titration, and the *black line* represents buffer-to-buffer titration. *Bottom panel*: *solid line* represents the one-site binding fitting of the ITC titration of IP_6 and indicated PH-TH domain. The experimental points are indicated in red square. The ITC titration of IP_3 and PH-TH^{E41K} domain could not be fit to any model. The plots were generated using Origin Pro 2020b. *B*, representative immunoblot of indicated mutants of full-length BTK with 100 µM IP_6. The level of autophosphorylation is determined with a total anti-phosphotyrosine antibody. *C*, densitometric analysis of the immunoblots in panel B. Data are presented as mean values ± SD from 5 to 7 independent experiments for E41K and 3 independent experiments for indicated double and triple mutants of PH-TH domain (E41K/R28H, E41K/R49S, E41K/R28H/R49S). An unpaired two-tailed *t* test was used to calculate significance. Data analyses were performed using GraphPad Prism version 9.5.1.

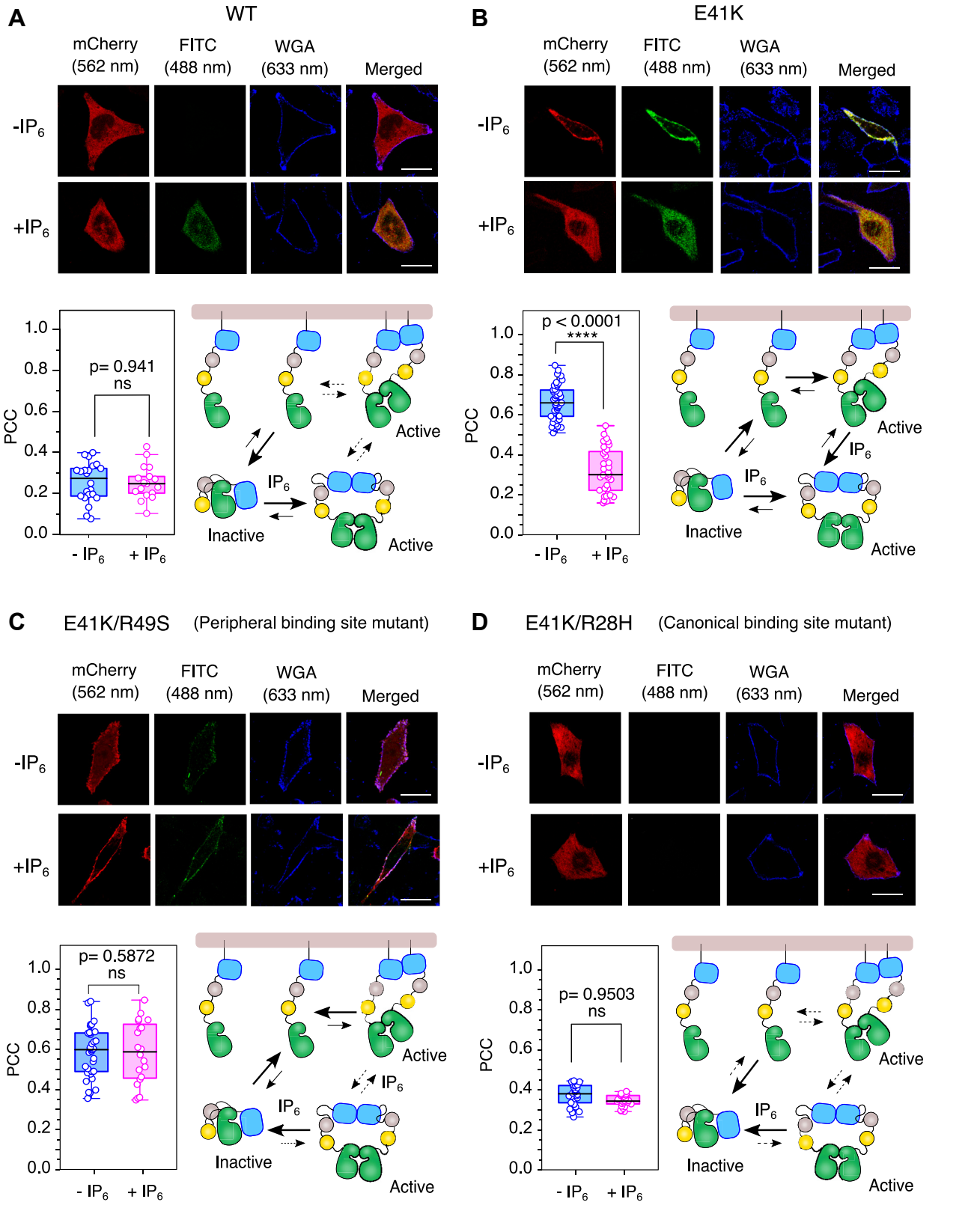

Figure 4. IP_6-dependent activation of BTK in CHO cell line. *A–D*, confocal images of transiently transfected BTK constructs fused to mCherry in CHO cell lines. The BTK expression level is shown in red (λ_{ex} = 552 nm, λ_{em} = 586–651 nm), and the phosphorylation status is shown in green (λ_{ex} = 488 nm, λ_{em} = 505–531 nm). The blue represents the plasma membrane stained with Wheat Germ Agglutinin (WGA) fused to Alexa 633 (λ_{ex} = 633 nm, λ_{em} = 647–692 nm). In each panel, the first column is the expression level of the indicated construct of BTK-mCherry. The second column represents the phosphorylation level Y551, determined with a specific anti-pY551 antibody followed by secondary staining with FITC conjugated secondary antibody. The third column shows the cell periphery (plasma membrane) labeled with WGA-Alexa633, and the last column is an overlay. The quantification of colocalization between BTK and WGA by Pearson's correlation coefficient (PCC) is shown in the bottom left of each panel. n = 22 to 25 over three independent experiments. scale bar = 30 μm. Boxplots represent quartiles. The data points outside the whisker range are set as outliers. The *black line* inside the box represents the median value. An unpaired two-tailed *t* test was used to calculate significance. Boxplots were generated using Origin Pro 2020b. Image analysis was done using Fiji Ver 1.54f. The bottom right in each panel shows the schematic model of BTK activation by IP_6.

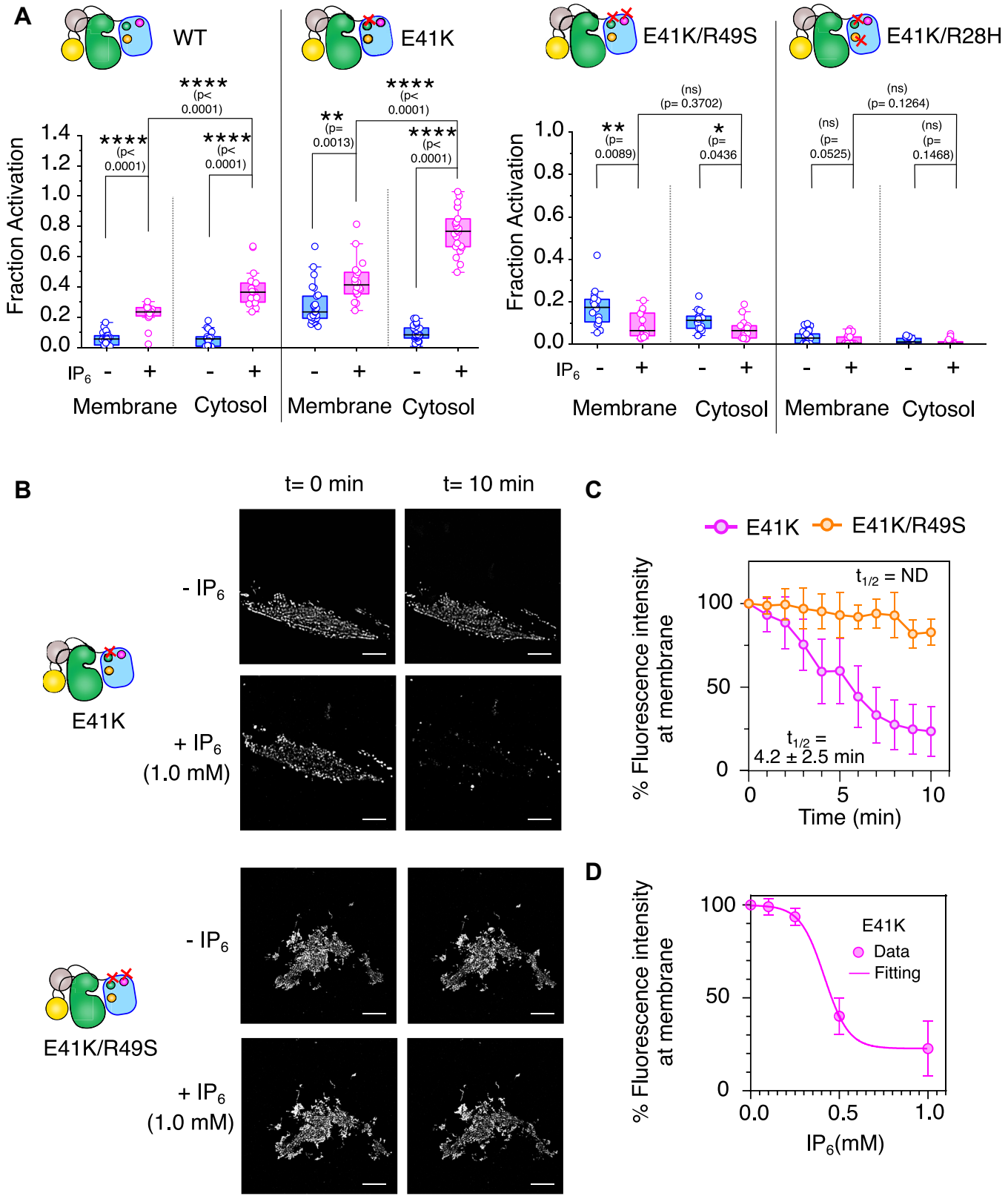

Figure 5. Determination of IP_6-dependent autophosphorylation and plasma membrane resident time of BTK. *A*, plots of fraction phosphorylated for the indicated BTK construct transiently expressed in CHO cell lines. The autophosphorylation level Y551 was determined with an anti-pY551 antibody. The phosphorylation of BTK localized at the plasma membrane and in the cytoplasm was measured in the presence and absence of IP_6. The fraction was obtained by normalizing the pY551 level (FITC intensity) by the BTK expression level (mCherry intensity). n = 22 to 25 cells over 5 independent experiments. Boxplots represent quartiles. The data points outside the whisker range are set as outliers. The *black line* inside the box represents the median value. An unpaired two-tailed *t* test was used to calculate significance. Boxplots were generated using Origin Pro 2020b. Image analysis was done using Fiji Ver 1.54f. *B*, representative Total Internal Reflection Fluorescence (TIRF) microscopy images of live CHO cells transiently transfected with BTK^{E41K} or $BTK^{E41K/R49S}$ mCherry in the presence or absence of 1 mM IP_6 at indicated time points. Scale bar = 10 μm. *C*, the fluorescence intensity at the plasma membrane

633 indicates plasma membrane boundary. We observed that IP_6 activates the cytosolic fraction of BTK wild-type (Figs. 4*A*, 5*A*, and S4*A*). This is consistent with previous reports (22, 33) that the wild-type BTK predominantly resides in the cytosol, which is activated by IP_6. In contrast, adding IP_6 significantly redistributes the membrane-bound fraction of BTK^{E41K} to the cytosol (Figs. 4*B* and S4*B*). The fraction of Y551 phosphorylation for the BTK^{E41K} mutant in the cytosol is now significantly higher than the membrane-bound fraction (Figs. 5*A* and S4*B*). The monomer control stays in the cytosol and cannot be activated by IP_6 stimulation (Figs. S3, *B–D* and S4*E*).

The TIRF imaging of the membrane-bound fraction of BTK^{E41K} shows that the IP_6 induces rapid redistribution of the kinase from the membrane to the cytosol with a $t_{1/2}$ of 4.2 ± 2.5 min (Fig. 5, *B* and *C*). The BTK^{E41K} mutant demonstrates an ultrasensitivity to IP_6 concentration. We observed that BTK^{E41K} remains at the membrane till 0.25 mM IP_6 concentration (Figs. 5*D* and S5). However, at a critical concentration of IP_6 (0.5 mM), the BTK^{E41K} comes out of the membrane. Our *in-vitro* studies showed that the mutation at the peripheral lipid binding site (R49S) of $PH\text{-}TH^{E41K}$ retains the ability to bind IP_6 to the canonical site (Fig. 3*A* and Table S1). We ask if full-length BTK bearing the same mutation could be activated in cells. We observed that the $BTK^{E41K/R49S}$ mutant remained at the membrane even after being stimulated with IP_6 and was weakly activated (Figs. 4*C* and S4*C*). Live cell imaging by TIRF microscopy shows that the $BTK^{E41K/R49S}$ mutant has a longer retention time at the plasma membrane, which does not come off the membrane after IP_6 stimulation throughout the duration of our experiment (Fig. 5, *B* and *C*). Our data indicates that the membrane-localized fraction of $BTK^{E41K/R49S}$ mutant dimerizes by binding PIP_3 to the intact canonical binding site. We could not detect the Y551 phosphorylation of $BTK^{E41K/R49S}$ mutant in the cytosolic fraction upon IP_6 stimulation (Figs. 4*C* and 5*A*). Together, this suggests that the binding of IP_6 to the peripheral site is critical for membrane-independent dimerization of BTK.

Our data suggests that the formation of the PH-TH Saraste dimer is crucial for BTK activation at the membrane or in the cytosol (30) (Fig. 6). However, the inability of IP_6 to peel the $BTK^{E41K/R49S}$ mutant from the plasma membrane indicates that the IP_6 may not be competing with the PIP_3 binding at the canonical lipid binding site. As anticipated, IP_6 stimulation does not activate $BTK^{E41K/R28H}$ mutated at the canonical binding site mutant (R28H) (Figs. 4*D* and 5*A*), suggesting that the two lipid-binding pockets of BTK are allosterically coupled to the Saraste dimer interface.

Conclusions

BTK is indispensable for B-lymphocyte development and proliferation, particularly during the maturation of the pre-B-cell stage to the mature stage (7). The PH-TH domain of BTK functions as a master regulator. The activating mutation (E41K) (47, 48) or loss of function mutant (XLA mutation) in the PH-TH domain leads to the manifestation of an immunodeficient phenotype (1, 2). The β3-β4 segment of PH-TH plays an important role in the allosteric crosstalk during the membrane recruitment and dimerization of the kinase (29, 30). One face of the β3-β4 segment constitutes the canonical lipid binding pocket for membrane localization (28). On the opposite side, the β3-β4 segment makes contact with an IP_6 molecule (22) and laterally interacts with the neighboring PH-TH domain. Therefore, mutation (such as E41K) that stabilizes the β3-β4 segment (lower B-factor) (37) enhances the structural stability of the PH-TH domain (Fig. 2*E*), thereby spontaneously activating the kinase.

Constitutive activation of BTK is often linked to several B-cell malignancies (7). Most BTK inhibitors are competitive inhibitors, competing for the ATP binding pocket. IP_6 is the only BTK activator reported in the literature. IP_6-mediated activation of BTK is distinct from IP_4, which works synergistically with the PIP_3 binding for the full activation of Tec family protein tyrosine kinases Itk (49). In contrast, it was speculated that the increased cellular concentration of IP_6 may outcompete the PIP_3 and PH-TH binding at the membrane and shift the equilibrium towards the cytosolic fraction (Fig. 4*B*) (22, 50). Counterintuitively, the IP_6 only perturbs the membrane localization of the BTK^{E41K} but not the peripheral binding site mutant (R49S) (Fig. 4*C*). Together, our data suggests that IP_6 may not compete with PIP_3 at the membrane to bind the PH-TH domain.

The crystal structure of the PH-TH domain in the complex with IP_6 (PDB ID: 4Y94) has four PH-TH domains present in the asymmetric unit (Fig. S6) (22). Two PH-TH domains are dimerized by the lateral interaction between the Saraste dimer interface (Fig. 2*A*) (28, 37). The Saraste dimer is compatible with the simultaneous PIP_3 binding to the canonical and the peripheral sites at the membrane (29, 30). An alternate homo dimer of PH-TH is also found (Fig. S6) at the asymmetric unit of the PH-TH domain structure (PDB ID: 4Y94). The PH-TH domain dimerizes by an asymmetric interaction between the adjacent β3-β4 segments, forming a pocket. One IP_6 molecule is sandwiched at the interface of two PH-TH domains, acting as a glue (Fig. 6). This dimer is only observed in the crystal structure of the IP_6:PH-TH complex and not in the presence of other inositol polyphosphate. Such an IP_6-dependent PH-TH dimer is incompatible with binding two PIP_3 molecules simultaneously to the canonical lipid binding site at the membrane while retaining the IP_6 molecule at the peripheral lipid binding site (Fig. 6). We speculate that IP_6 may stabilize the alternate dimer over the Saraste dimer. Thus, shifting the equilibrium to the alternate PH-TH dimer, thereby dislodging the BTK^{E41K} from the plasma membrane (Figs. 4*B* and 5*B*).

measured in the transiently transfected live CHO cells with the indicated BTK-mCherry constructs following IP_6 stimulation is plotted as a function of time. Data are presented as mean values ± SD from three independent experiments. Data analyses were performed using GraphPad Prism version 9.5.1. The $t_{1/2}$ is determined by fitting the decay of the fluorescence intensity to exponential decay. Image analysis was done using Fiji Ver 1.54f. *D*, the plot of fluorescence intensity of BTK^{E41K} mCherry against indicated IP_6 concentration. Data are presented as mean values ± SD from three independent experiments. Data analyses were performed using GraphPad Prism version 9.5.1. Image analysis was done using Fiji Ver 1.54f.

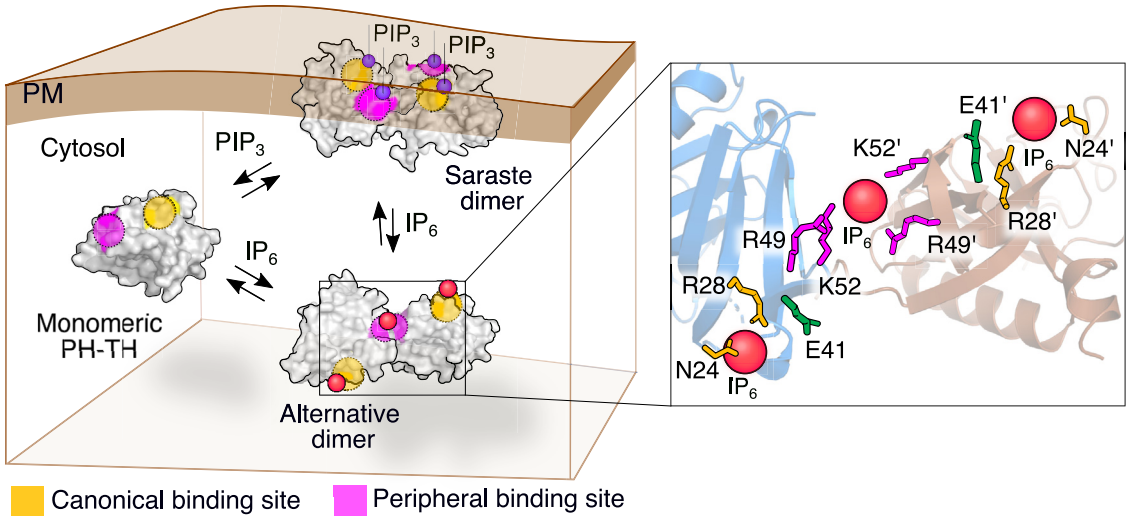

Figure 6. The proposed model for the IP_6-dependent dimerization of the PH-TH domain. In the absence of stimulation, the PH-TH domain remains in solution as a monomer. The binding of PIP_3 at the canonical site recruits BTK to the membrane and the Saraste dimer interface is stabilized by PIP_3 binding to the peripheral site. The canonical and peripheral lipid binding sites are indicated with *yellow* and *magenta*, respectively. IP_6 promotes an alternate dimer of the PH-TH domain, shifting the equilibrium to a PH-TH dimer in solution. The residues in the canonical and peripheral binding sites are shown in the inset. The IP_6 molecules are indicated by *red balls*.

The peripheral site mutant (R49S) cannot form the alternate dimer and remains at the plasma membrane even in the presence of IP_6 (Fig. 4*C*). The ultrasensitivity of BTK^{E41K} to the IP_6 concentration (Fig. 5*D*) indicates that the PH-TH functions as a switch that, at a critical IP_6 concentration, toggles the PH-TH Saraste dimer to the alternate dimer (30).

Our data show that the XLA mutation (R28H) impairs dimerization of the PH-TH domain and IP_6-dependent phosphorylation of Y551 of BTK (Figs. 4*D* and S3D). The R28H mutation may have impaired response to the T-cell-independent B-cell antigens, explaining why patients with XLA are more susceptible to recurring bacterial and viral infection (1–4). We speculate that the ability of IP_6 to activate BTK independent of BCR activation in our experiment opens a new opportunity to develop immune modulators.

Experimental procedures

Constructs

The PH-TH domain of BTK wildtype (amino acid residue number 4–170) cloned into pET28-SUMO vector was gifted from Prof John Kuriyan, UC Berkeley. The pMSCV-BTK-mCherry construct was a gift from Hidde Ploegh (Addgene plasmid #50043). The full-length BTK was cloned into the pET28-SUMO vector. For the microscopy studies, the BTK-mCherry was cloned into a pCDNA vector. The point mutations in all the constructs were done by site-directed mutagenesis.

Expression and purification of BTK PH-TH domain

The PH-TH domain of BTK cloned into pET28-SUMO vector was expressed in *E.coli* BL21-DE3 cells by inducing with 1 mM IPTG and at 18°C for overnight (22). The cells were lysed in lysis buffer (25 mM Tris-Cl, 500 mM NaCl, 20 mM Imidazole, 5% Glycerol, 2 mM β-ME, pH 8.5). The protein was purified using a Ni-NTA column, and buffer exchanged to 25 mM Tris-Cl, 400 mM NaCl pH 8. His tag was removed by incubating with ULP1 protease for 12 h, and the PH-TH domain was further purified by gel filtration chromatography. the protein was concentrated and stored at −80°C.

Expression and Purification of full length BTK

The full-length BTK cloned in pET28-SUMO vector was co-transformed with YopH and Trigger factor in *E.coli* BL21-DE3 cells (22). Briefly, the cells were grown in LB supplemented with 50 mg/ml Kanamycin, 35 μg/ml chloramphenicol, and 50 μg/ml streptomycin. The BTK expression was induced with 1 mM IPTG and was grown at 18 °C for 16 h. The cells were lysed in lysis buffer (25 mM Tris-Cl, 500 mM NaCl, 20 mM Imidazole, 5% Glycerol, 2 mM β-ME, pH 8.5) and the protein was purified using Ni-NTA column. His tag was removed by digesting BTK with ULP1 protease for 12 h. The undigested protein was then removed by passing through the second Ni-NTA column and the flow through was concentrated and stored at −80 °C.

Isothermal titration calorimetry

The isothermal titration calorimetry experiments were performed using MicroCal ITC (GE Healthcare) and MicroCal PEAQ-ITC (Malvern). The PH-TH domain was buffer exchanged to 20 mM HEPES, 150 mM NaCl, pH 7.5. During the titration, 25 μM protein in the cell was titrated with a ligand at the protein-to-ligand ratio of 1: 5.5. All ITC titrations were performed at 20 °C. The initial injection of 0.5 μl was excluded from the data analysis. During the titration, 3 μl of ligand was injected in 13 steps, and each injection step was separated by 180 s. The protein solution was stirred at 300 rpm during the titration.

Size-exclusion chromatography

Size-exclusion chromatography of various constructs of the PH-TH domain was performed using the Superdex-200

10/300 Gl column. For the apo PH-TH domain, the column was equilibrated with running buffer (25 mM Tris-Cl, 100 mM NaCl, 1 mM DTT, pH 7.2), and 500 µl of 75 µM protein was loaded into the column, at a flow rate of 0.3 ml/min and at 8 °C. The elution profile was recorded, and the retention time of the protein was calculated. For the ligand-bound samples, the protein was mixed with ligand at a protein-to-ligand ratio of 1:4, and incubated at 4 °C for 15 min before loading into the size-exclusion column. Before loading the sample, the column was pre-equilibrated with a running buffer containing the ligand.

Dynamic light scattering

The Dynamic Light Scattering experiments were conducted using Malvern Zetasizer DLS Detectors using 1.5 ml plastic cuvettes. The samples were prepared in a buffer containing 25 mM Tris-Cl, 100 mM NaCl, 1 mM DTT, and pH 7.2. The experiment included three measurements of ten runs each. The theoretical calculations of the hydrodynamic radius of the proteins were performed using Hydropro (51).

Thermal denaturation by circular dichroism spectroscopy

The melting temperature of the PH-TH domain was determined from the Circular Dichroism (CD) spectrum recorded at increasing temperatures (20° to 76 °C). For each sample, the CD spectra from 300 to 190 nm were recorded using a Jasco-J1500 spectropolarimeter with a temperature increment of 4 °C. CD spectra were recorded with 5 µM protein in 20 mM Sodium phosphate buffer pH 7.4 and in the absence or in the presence of an equimolar ligand. The measured ellipticity data was converted into molar ellipticity (39).

The $\Delta G_{Unfolding}$ was calculated considering the simplest two-step unfolding model, where a protein exists in a folded (F) and an unfolded (U) state as described previously (40, 41). The fraction unfolded [U] protein at a given temperature is:

$$[U] = \frac{(\theta_T - \theta_F)}{(\theta_U - \theta_F)} \quad (1)$$

Where, θ_F and θ_U are the molar ellipticity of the fully folded and unfolded state at 218 nm, θ_T is the molar ellipticity at a given temperature. Considering that at a given temperature, the sum of the unfolded and folded [F] fraction of the protein is 1, the equilibrium constant, $K_{Unfolding}$ is:

$$K_{Unfolding} = \frac{[U]}{1-[U]} \quad (2)$$

Thus, free energy of unfolding was derived using $\Delta G_{Unfolding} = -RTln(K_{Unfolding})$, where R is the universal gas constant (1.98 cal $mol^{-1}K^{-1}$). The $\Delta\Delta G_{unfolding}$ was calculated from the difference between the ΔG of the IP_6 bound ΔG_{holo} and ΔG_{apo} state, measured at the T_m of the corresponding apo PH-TH construct.

Autophosphorylation assay by immunoblot

The activation of full-length BTK in response to the ligand was determined from the autophosphorylation Y551 or total phosphotyrosine level. Before each reaction, 2 µM BTK was incubated with 100 µM ligand for 10 min. The phosphorylation reaction was performed at 25 °C in a buffer containing 25 mM Tris-Cl (pH 7.5), 2 mM ATP, 10 mM $MgCl_2$, and 1 mM Na_3VO_4. The reaction was quenched with SDS–PAGE loading buffer. The autophosphorylation levels of full-length BTK were detected by immunoblot (22). The amount of BTK loaded was determined using an anti-BTK antibody. Densitometric analysis of immunoblots was performed using Fiji software (52).

Cell-based assay

The IP_6-mediated activation of BTK was determined by immunofluorescence and immunoblot in Chinese Hamster Ovary (CHO) cell line transiently transfected with BTK-mCherry cloned in pCDNA. The CHO cell line was obtained from the National Center for Cell Science cell repository in Pune, India, and tested for *mycoplasma* contamination. Before activation, transfected cells were serum-starved for 6 h in opti-MEM, followed by incubation with 500 µM IP_6 for 1 h in opti-MEM. For Immunoblot, cells were washed with ice-cold PBS and then incubated in RIPA buffer [10 mM Tris-Cl (pH 8.0), 140 mM NaCl, 1 mM EDTA, 0.1% SDS, and 1% Triton X-100] containing protease and phosphatase inhibitors (2 mM Benzamidine, 1 mM PMSF and 1 mM Sodium orthovanadate) for 10 min. The cell lysates were sonicated, and protein samples were prepared by heating with 5X loading buffer and resolved in a 6% SDS-PAGE. Protein samples were transferred onto the PVDF membrane at 15 V for 1 h, followed by blocking with 5% skimmed milk in 1X TBS containing 0.1% TWEEN-20 for 1 h at room temperature. After blocking, the blot was incubated overnight at 4 °C with the primary antibody (1:1000) diluted in 3% skimmed milk. After incubation, the blot was washed three times with 1X TBST (0.1% TWEEN-20), followed by incubation with a secondary antibody (1:2000) diluted in 3% skimmed milk. Blots were washed three times with 1X TBST and developed using the Clarity Western ECL substrate kit (Bio-Rad). Densitometry analysis of immunoblots was performed using Fiji Ver 1.54f (52).

For the immunofluorescence study, Cells were washed with PBS once, followed by incubation with WGA (20 µg/ml) in PBS at 37 °C for 1 min. After incubation, cells were washed with PBS and immediately fixed with 4% paraformaldehyde in PBS for 30 min at room temperature. After fixation, cells were washed five times with 1x PBS and permeabilized with 0.2% PBST for 5 min at room temperature. Cells were blocked with 1% BSA for 1 h at room temperature, followed by staining with anti-551pY primary antibody (1:100 dilution) in blocking buffer overnight at 4 °C. After incubation, cells were incubated with a FITC-conjugated secondary antibody in a blocking buffer for 2 h at room temperature. Finally, coverslips were

mounted with prolonged gold. Coverslips were washed three times with 1X PBS in between each step. Details of the antibody used are summarized in Table S3.

Confocal microscopy and image analysis

All images were acquired with the Leica SP8 confocal platform using an oil immersion HC PL APO CS2 63 × objective (NA 1.4) at 3.0X digital zoom. Image scanning was done in bidirectional mode at 500 Hz. The level of BTK on the membrane or cytoplasm was determined from the intensity of mCherry measured at λ_{ex} = 552 nm and λ_{em} = 576 to 651 nm, respectively. The Y551 phosphorylation was determined from the intensity of FITC tagged to the secondary antibody and measured at λ_{ex} = 488 nm and λ_{em} = 505 to 531 nm. The plasma membrane was stained with Wheat Germ Agglutinin (WGA) fused to Alexa 633 and imaged at λ_{ex} = 633 nm, λ_{em} = 647 to 692 nm, respectively. ROIs were drawn manually using the Fiji freehand tool (Ver 1.54f) (52). ROI1 marked the outer boundary of the cell perimeter labeled with WGA, ROI2 marked the inner boundary of the cell perimeter, and ROI3 marked the nucleus. The ROI1 provides the total cell intensity. The intensity of mCherry or FITC at the membrane was determined by subtracting the respective intensities of ROI2 from ROI1. Whereas cytoplasmic intensity of mCherry or FITC was determined by subtracting the respective intensities of ROI3 from ROI2. The membrane localization of the BTK-mCherry construct was determined from the quantification of Pearson's colocalization coefficient (PCC) (45).

Total internal reflection fluorescence (TIRF) microscopy

For Total internal reflection fluorescence (TIRF) microscopy, CHO cells were seeded in a glass bottom dish and transfected with 500 ng DNA. After 16 h of post-transfection, cells were serum starved by incubating in Opti-MEM serum-free media for 6 h. The images of lived CHO cells were recorded for 10 min before and after IP_6 treatment. The TIRF images were acquired on a Nikon Eclipse Ti2 inverted microscope equipped with a Nikon 100 × 1.49 numerical aperture oil-immersion TIRF objective, a TIRF illuminator, a Perfect Focus system (PFS), and a motorized stage. The critical angle and the refractive index were set to 63° and 1.515, respectively (53). The samples were excited at 561 nm using an LU-N4 laser unit (Nikon, Tokyo, Japan) with solid-state lasers. Image acquisition was done using the Nikon NIS-Elements software. Live cell images were acquired at 1-min intervals for 10 min using an EMCCD camera, with an exposure time of 200 ms.

The images were processed and analyzed using Fiji. Out-of-focus fluorescence in the acquired images is removed by deconvolution (54). Image ROIs were drawn using the elliptical tool for each cell. The fluorescence intensity of each frame was quantified using "create spectrum jru V1" routine of Fiji. The half-life of fluorescence intensity at the plasma membrane was determined by fitting the fluorescence decay at indicated time points to a first-order kinetic equation using GraphPad Prism version 9.5.1.

Analysis of intracellular IP_6 by NMR spectroscopy

The intracellular IP_6 was extracted with TiO_2 (55) and analyzed by NMR spectroscopy (56). Briefly, CHO cells were grown to a confluency of 2.6 × 10^7 cells at 37 °C and 5% CO_2. Before IP_6 treatment, cells were serum starved for 6 h, and then 5 mM IP_6 in 25 mM Tris buffer (pH 7.4) was added and incubated for 30 min. The cells were then washed twice with ice-cold PBS to remove excess IP_6 and lysed by incubating with ice-cold 1M Perchloric acid for 10 min. The cell extract was centrifuged at 14,000*g* for 10 min to remove the cell debris. The TiO_2 slurry was prepared by washing 200 mg of TiO_2 powder with 5 ml of deionized water and then resuspended in 1M Perchloric acid. The cell extracted in perchloric acid was added to the TiO_2 and incubated at 4 °C for 15 min. The supernatant was removed by centrifugation, and the bound phosphate compounds were eluted from TiO_2 with 2.8% NH_4OH. The eluate was lyophilized overnight and resuspended in a Sodium Phosphate buffer (pH 6.5) containing 50 mM KCl. The sample was again lyophilized to remove any residual water and resuspended in 100% D_2O for the NMR analysis. Commercially purchased pure IP_6 was used as a standard. The 1D proton NMR spectrum was recorded at a ^1H frequency of 500 MHz. The relaxation delay was set at 5 s and the spectral width of 12,500 Hz. The data was analyzed with Bruker Topspin 4.4.0.

Data availability

All the relevant data are contained within this article and in the supporting information.

Supporting information—This article contains supporting information.

Acknowledgments—The authors thank Prof Arnab Gupta for access to the confocal microscope and Prosad Kumar Das for his valuable input.

Author contributions—B. P. D., K. G., M. P. C., S. R., and S. C. writing–review & editing; B. P. D., K. G., M. P. C., S. R., and S. C. methodology; B. P. D., K. G., M. P. C., S. R., and S. C. formal analysis; K. G., M. P. C., S. C., and R. D. writing–original draft; M. P. C., S. R., and S. C. investigation; M. P. C., S. R., and S. C. data curation; M. P. C., S. C., and R. D. conceptualization. R. D. supervision; R. D. resources; R. D. project administration; R. D. funding acquisition.

Funding and additional information—The authors thank research funding from IISER Kolkata, infrastructural facilities supported by IISER Kolkata, and DST-FIST (SR/FST/LS-II/2017/93(c)). This work is supported by grants from SERB (ECR/2015/000142) and (CRG/2020/000437).

Conflict of interest—The authors declare that they have no conflict of interest with the contents of this article.

Abbreviations—The abbreviations used are: BCR, B-cell receptor; BTK, Bruton's tyrosine kinase; IP6, inositol hexakisphosphate; PH, pleckstrin homology; PIP3, phosphatidylinositol 3–5-triphosphate; TH, Tec homology; TI, T-cell-independent; TIRF, Total internal reflection fluorescence; XLA, X-linked agammaglobulinemia.

References

1. Tsukada, S., Saffran, D. C., Rawlings, D. J., Parolini, O., Allen, R. C., Klisak, I., *et al.* (1993) Deficient expression of a B cell cytoplasmic tyrosine kinase in human X-linked agammaglobulinemia. *Cell* **72**, 279–290
2. Vetrie, D., Vorechovsky, I., Sideras, P., Holland, J., Davies, A., Flinter, F., *et al.* (1993) The gene involved in X-linked agammaglobulinaemia is a member of the src family of protein-tyrosine kinases. *Nature* **361**, 226–233
3. Thomas, J. D., Sideras, P., Smith, C. I., Vorechovsky, I., Chapman, V., and Paul, W. E. (1993) Colocalization of X-linked agammaglobulinemia and X-linked immunodeficiency genes. *Science* **261**, 355–358
4. Fukuda, M., Kojima, T., Kabayama, H., and Mikoshiba, K. (1996) Mutation of the pleckstrin homology domain of Bruton's tyrosine kinase in immunodeficiency impaired inositol 1, 3, 4, 5-tetrakisphosphate binding capacity. *J. Biol. Chem.* **271**, 30303–30306
5. Woyach, J. A., Bojnik, E., Ruppert, A. S., Stefanovski, M. R., Goettl, V. M., Smucker, K. A., *et al.* (2014) Bruton's tyrosine kinase (BTK) function is important to the development and expansion of chronic lymphocytic leukemia (CLL). *Blood* **123**, 1207–1213
6. Davis, R. E., Ngo, V. N., Lenz, G., Tolar, P., Young, R. M., Romesser, P. B., *et al.* (2010) Chronic active B-cell-receptor signalling in diffuse large B-cell lymphoma. *Nature* **463**, 88–92
7. Hendriks, R. W., Yuvaraj, S., and Kil, L. P. (2014) Targeting Bruton's tyrosine kinase in B cell malignancies. *Nat. Rev. Cancer* **14**, 219–232
8. Joseph, R. E., Amatya, N., Fulton, D. B., Engen, J. R., Wales, T. E., and Andreotti, A. (2020) Differential impact of BTK active site inhibitors on the conformational state of full-length BTK. *Elife* **9**, e60470
9. Byrd, J. C., Furman, R. R., Coutre, S. E., Flinn, I. W., Burger, J. A., Blum, K. A., *et al.* (2013) Targeting BTK with ibrutinib in relapsed chronic lymphocytic leukemia. *N. Engl. J. Med.* **369**, 32–42
10. Wang, M. L., Rule, S., Martin, P., Goy, A., Auer, R., Kahl, B. S., *et al.* (2013) Targeting BTK with ibrutinib in relapsed or refractory mantle-cell lymphoma. *N. Engl. J. Med.* **369**, 507–516
11. Lee, K. G., Xu, S., Kang, Z. H., Huo, J., Huang, M., Liu, D., *et al.* (2012) Bruton's tyrosine kinase phosphorylates Toll-like receptor 3 to initiate antiviral response. *Proc. Natl. Acad. Sci. U. S. A.* **109**, 5791–5796
12. Desiderio, S. (1997) Role of Btk in B cell development and signaling. *Curr. Opin. Immunol.* **9**, 534–540
13. Wahl, M. I., Fluckiger, A. C., Kato, R. M., Park, H., Witte, O. N., and Rawlings, D. J. (1997) Phosphorylation of two regulatory tyrosine residues in the activation of Bruton's tyrosine kinase via alternative receptors. *Proc. Natl. Acad. Sci. U. S. A.* **94**, 11526–11533
14. Salim, K., Bottomley, M. J., Querfurth, E., Zvelebil, M., Gout, I., Scaife, R., *et al.* (1996) Distinct specificity in the recognition of phosphoinositides by the pleckstrin homology domains of dynamin and Bruton's tyrosine kinase. *EMBO J.* **15**, 6241–6250
15. Rawlings, D. J., and Witte, O. N. (1995) The Btk subfamily of cytoplasmic tyrosine kinases: structure, regulation and function. *Semin. Immunol.* **7**, 237–246
16. Nagar, B., Hantschel, O., Young, M. A., Scheffzek, K., Veach, D., Bornmann, W., *et al.* (2003) Structural basis for the autoinhibition of c-Abl tyrosine kinase. *Cell* **112**, 859–871
17. Xu, W., Harrison, S. C., and Eck, M. J. (1997) Three-dimensional structure of the tyrosine kinase c-Src. *Nature* **385**, 595–602
18. Sicheri, F., Moarefi, I., and Kuriyan, J. (1997) Crystal structure of the Src family tyrosine kinase Hck. *Nature* **385**, 602–609
19. Sideras, P., and Smith, C. I. (1995) Molecular and cellular aspects of X-linked agammaglobulinemia. *Adv. Immunol.* **59**, 135–223
20. Mohamed, A. J., Yu, L., Backesjo, C. M., Vargas, L., Faryal, R., Aints, A., *et al.* (2009) Bruton's tyrosine kinase (Btk): function, regulation, and transformation with special emphasis on the PH domain. *Immunol. Rev.* **228**, 58–73
21. Joseph, R. E., Min, L., and Andreotti, A. H. (2007) The linker between SH2 and kinase domains positively regulates catalysis of the Tec family kinases. *Biochemistry* **46**, 5455–5462
22. Wang, Q., Vogan, E. M., Nocka, L. M., Rosen, C. E., Zorn, J. A., Harrison, S. C., *et al.* (2015) Autoinhibition of Bruton's tyrosine kinase (Btk) and activation by soluble inositol hexakisphosphate. *Elife* **4**, e06074
23. Devkota, S., Joseph, R. E., Boyken, S. E., Fulton, D. B., and Andreotti, A. H. (2017) An autoinhibitory role for the pleckstrin homology domain of Interleukin-2-Inducible tyrosine kinase and its Interplay with canonical Phospholipid recognition. *Biochemistry* **56**, 2938–2949
24. Amatya, N., Wales, T. E., Kwon, A., Yeung, W., Joseph, R. E., Fulton, D. B., *et al.* (2019) Lipid-targeting pleckstrin homology domain turns its autoinhibitory face toward the TEC kinases. *Proc. Natl. Acad. Sci. U. S. A.* **116**, 21539–21544
25. Joseph, R. E., Wales, T. E., Fulton, D. B., Engen, J. R., and Andreotti, A. H. (2017) Achieving a Graded immune response: BTK adopts a range of active/Inactive conformations Dictated by Multiple Interdomain contacts. *Structure* **25**, 1481–1494.e1484
26. Aoki, Y., Isselbacher, K. J., and Pillai, S. (1994) Bruton tyrosine kinase is tyrosine phosphorylated and activated in pre-B lymphocytes and receptor-ligated B cells. *Proc. Natl. Acad. Sci. U. S. A.* **91**, 10606–10609
27. de Weers, M., Brouns, G. S., Hinshelwood, S., Kinnon, C., Schuurman, R. K., Hendriks, R. W., *et al.* (1994) B-cell antigen receptor stimulation activates the human Bruton's tyrosine kinase, which is deficient in X-linked agammaglobulinemia. *J. Biol. Chem.* **269**, 23857–23860
28. Hyvonen, M., and Saraste, M. (1997) Structure of the PH domain and Btk motif from Bruton's tyrosine kinase: molecular explanations for X-linked agammaglobulinaemia. *EMBO J.* **16**, 3396–3404
29. Wang, Q., Pechersky, Y., Sagawa, S., Pan, A. C., and Shaw, D. E. (2019) Structural mechanism for Bruton's tyrosine kinase activation at the cell membrane. *Proc. Natl. Acad. Sci. U. S. A.* **116**, 9390–9399
30. Chung, J. K., Nocka, L. M., Decker, A., Wang, Q., Kadlecek, T. A., Weiss, A., *et al.* (2019) Switch-like activation of Bruton's tyrosine kinase by membrane-mediated dimerization. *Proc. Natl. Acad. Sci. U. S. A.* **116**, 10798–10803
31. Park, H., Wahl, M. I., Afar, D. E., Turck, C. W., Rawlings, D. J., Tam, C., *et al.* (1996) Regulation of Btk function by a major autophosphorylation site within the SH3 domain. *Immunity* **4**, 515–525
32. Rawlings, D. J., Scharenberg, A. M., Park, H., Wahl, M. I., Lin, S., Kato, R. M., *et al.* (1996) Activation of BTK by a phosphorylation mechanism initiated by SRC family kinases. *Science* **271**, 822–825
33. Kim, W., Kim, E., Min, H., Kim, M. G., Eisenbeis, V. B., Dutta, A. K., *et al.* (2019) Inositol polyphosphates promote T cell-independent humoral immunity via the regulation of Bruton's tyrosine kinase. *Proc. Natl. Acad. Sci. U. S. A.* **116**, 12952–12957
34. Saiardi, A., Erdjument-Bromage, H., Snowman, A. M., Tempst, P., and Snyder, S. H. (1999) Synthesis of diphosphoinositol pentakisphosphate by a newly identified family of higher inositol polyphosphate kinases. *Curr. Biol.* **9**, 1323–1326
35. Li, T., Tsukada, S., Satterthwaite, A., Havlik, M. H., Park, H., Takatsu, K., *et al.* (1995) Activation of Bruton's tyrosine kinase (BTK) by a point mutation in its pleckstrin homology (PH) domain. *Immunity* **2**, 451–460
36. Kanegane, H., Futatani, T., Wang, Y., Nomura, K., Shinozaki, K., Matsukura, H., *et al.* (2001) Clinical and mutational characteristics of X-linked agammaglobulinemia and its carrier identified by flow cytometric assessment combined with genetic analysis. *J. Allergy Clin. Immunol.* **108**, 1012–1020
37. Baraldi, E., Carugo, K. D., Hyvönen, M., Surdo, P. L., Riley, A. M., Potter, B. V., *et al.* (1999) Structure of the PH domain from Bruton's tyrosine kinase in complex with inositol 1, 3, 4, 5-tetrakisphosphate. *Structure* **7**, 449–460
38. Várnai, P., Rother, K. I., and Balla, T. (1999) Phosphatidylinositol 3-kinase-dependent membrane association of the Bruton's tyrosine kinase pleckstrin homology domain visualized in single living cells. *J. Biol. Chem.* **274**, 10983–10989

39. Greenfield, N. J. (2006) Using circular dichroism collected as a function of temperature to determine the thermodynamics of protein unfolding and binding interactions. *Nat. Protoc.* **1**, 2527–2535
40. Robertson, A. D., and Murphy, K. P. (1997) Protein structure and the Energetics of protein stability. *Chem. Rev.* **97**, 1251–1268
41. Greenfield, N. J. (2006) Analysis of the kinetics of folding of proteins and peptides using circular dichroism. *Nat. Protoc.* **1**, 2891–2899
42. de Weers, M., Mensink, R. G., Kraakman, M. E., Schuurman, R. K., and Hendriks, R. W. (1994) Mutation analysis of the Bruton's tyrosine kinase gene in X-linked agammaglobulinemia: identification of a mutation which affects the same codon as is altered in immunodeficient xid mice. *Hum. Mol. Genet.* **3**, 161–166
43. Saouaf, S. J., Mahajan, S., Rowley, R. B., Kut, S. A., Fargnoli, J., Burkhardt, A. L., *et al.* (1994) Temporal differences in the activation of three classes of non-transmembrane protein tyrosine kinases following B-cell antigen receptor surface engagement. *Proc. Natl. Acad. Sci. U. S. A.* **91**, 9524–9528
44. Chazotte, B. (2011) Labeling membrane glycoproteins or glycolipids with fluorescent wheat germ agglutinin. *Cold Spring Harb. Protoc.* **2011**, pdb.prot5623
45. Kar, S., Sen, S., Maji, S., Saraf, D., Ruturaj, Paul, R., *et al.* (2022) Copper(II) import and reduction are dependent on His-Met clusters in the extracellular amino terminus of human copper transporter-1. *J. Biol. Chem.* **298**, 101631
46. Vucenik, I., and Shamsuddin, A. M. (1994) [3H]inositol hexaphosphate (phytic acid) is rapidly absorbed and metabolized by murine and human malignant cells in vitro. *J. Nutr.* **124**, 861–868
47. Maas, A., Dingjan, G. M., Grosveld, F., and Hendriks, R. W. (1999) Early arrest in B cell development in transgenic mice that express the E41K Bruton's tyrosine kinase mutant under the control of the CD19 promoter region. *J. Immunol.* **162**, 6526–6533
48. Dingjan, G. M., Maas, A., Nawijn, M. C., Smit, L., Voerman, J. S., Grosveld, F., *et al.* (1998) Severe B cell deficiency and disrupted splenic architecture in transgenic mice expressing the E41K mutated form of Bruton's tyrosine kinase. *EMBO J.* **17**, 5309–5320
49. Huang, Y. H., Grasis, J. A., Miller, A. T., Xu, R., Soonthornvacharin, S., Andreotti, A. H., *et al.* (2007) Positive regulation of Itk PH domain function by soluble IP4. *Science* **316**, 886–889
50. Chakraborty, A., Koldobskiy, M. A., Bello, N. T., Maxwell, M., Potter, J. J., Juluri, K. R., *et al.* (2010) Inositol pyrophosphates inhibit Akt signaling, thereby regulating insulin sensitivity and weight gain. *Cell* **143**, 897–910
51. Ortega, A., Amorós, D., and De La Torre, J. G. (2011) Prediction of hydrodynamic and other solution properties of rigid proteins from atomic- and residue-level models. *Biophys. J.* **101**, 892–898
52. Schindelin, J., Arganda-Carreras, I., Frise, E., Kaynig, V., Longair, M., Pietzsch, T., *et al.* (2012) Fiji: an open-source platform for biological-image analysis. *Nat. Methods* **9**, 676–682
53. Fish, K. N. (2009) Total internal reflection fluorescence (TIRF) microscopy. *Curr. Protoc. Cytom.* **Chapter 12**. Unit12 18
54. Liao, P. C., Yang, E. J., and Pon, L. A. (2020) Live-cell imaging of Mitochondrial redox state in Yeast cells. *STAR Protoc.* **1**, 100160
55. Wilson, M. S., and Saiardi, A. (2018) Inositol phosphates Purification using Titanium Dioxide Beads. *Bio Protoc.* **8**, e2959
56. Ouyang, Z., Zheng, G., Tomchick, D. R., Luo, X., and Yu, H. (2016) Structural basis and IP6 Requirement for Pds5-dependent Cohesin dynamics. *Mol. Cell* **62**, 248–259